Photochemical & Photobiological Sciences (2021) 20:501–512
https://doi.org/10.1007/s43630-021-00030-0

ORIGINAL PAPERS

4-Hydroxyl-oxoisoaporphine, one small molecule as theranostic agent for simultaneous fluorescence imaging and photodynamic therapy as type II photosensitizer

Qi Xu[1] · Yunfan Ji[1] · Meijun Chen[1] · Xusheng Shao[1,2]

Received: 18 November 2020 / Accepted: 17 February 2021 / Published online: 20 March 2021

Abstract

Oxoisoaporphine (OA) is a plant phototoxin isolated from *Menispermaceae*, however, its weak fluorescence and low water solubility impede it for theranostics. We developed here 4-hydroxyl-oxoisoaporphine (OHOA), which has good singlet oxygen-generating ability (0.06), strong fluorescence (0.72) and improved water solubility. OHOA displays excellent fluorescence for cell imaging and exhibits light-induced cytotoxicity against cancer cell. In vitro model of human cervical carcinoma (HeLa) cell proved that singlet oxygen generated by OHOA triggered photosensitized oxidation reactions and exert toxic effect on tumor cells. The MTT assay using HeLa cells verified the low cytotoxicity of OHOA in the dark and high phototoxicity. Confocal experiment indicates that OHOA mainly distributes in mitochondria and western blotting demonstrated that OHOA induces cell apoptosis via the mitochondrial pathway in the presence of light. Our molecule provides an alternative choice as a theranostic agent against cancer cells which usually are in conflict with each other for most traditional theranostic agents.

Graphic abstract

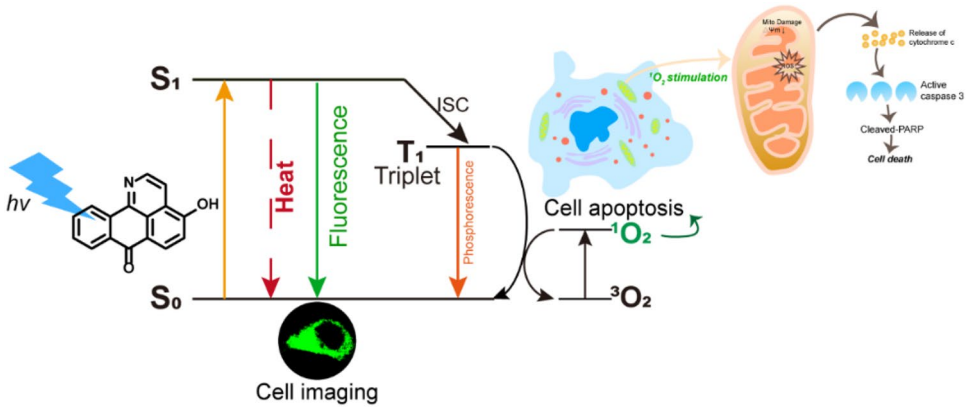

Keywords Oxoisoaporphine · Photosensitizer · Cell imaging · Singlet oxygen · Cytotoxicity

✉ Xusheng Shao
shaoxusheng@ecust.edu.cn

[1] Shanghai Key Laboratory of Chemical Biology, School of Pharmacy, East China University of Science and Technology, Shanghai 200237, China

[2] State Key Laboratory of Bioreactor Engineering, East China University of Science and Technology, Shanghai 200237, China

1 Introduction

Photodynamic therapy (PDT) has attracted tremendous attention due to its non-invasive nature and high specificity for cancer treatment [1–3]. This technology utilizes singlet oxygen ($^1O_2$) generated by photosensitizers (PS) when absorb specific wavelengths of light, causing oxidative stress

on tissues and abnormal proliferation of active cells [4–6]. This results in irreversible cellular damage and subsequent cell death [7]. PS is the key for successful implementation of PDT. The most attractive characteristic of PDT is its lasting selectivity as photodynamic effect happens only where the PSs accumulated and where the light is applied. However, the short-lived $^1O_2$ (3 µs) will not migrate more than a fraction of a micron from its site of formation (20 nm) [8]. Therefore, photosensitizers located in the organelles have a more effective photodynamic effect [9–12]. Developing a photosensitizer with excellent singlet oxygen-generating ability, good photostability and biologically benign absorption band is urgent. Furthermore, some processes of photosensitizer activation are accompanied by the generation of fluorescence and phosphorescence, which means a theragnostic effect can be achieved on a single molecule [13–15].

Phenalenones (PNs) is a kind of phytoalexins synthesized de novo by plants and accumulated rapidly at areas of pathogen infection, which is produced at the first stage of black sigatoka that *Mycosphaerella fijensis* infected banana trees. PN is known to be an efficient type II photosensitizer that can produce equivalent singlet oxygen upon light irradiation against mosquito and nematode [16–18]. Compounds with a structure based on the PN skeleton are effective type II photosensitizers for fast killing of key oral pathogens, in particular, drug-resistant bacteria [19]. We previously found that PN derivatives exhibited light-induced $^1O_2$-mediated lethal activity against mosquito larvae and root-knot nematode [20].

Isoquinoline alkaloid oxoisoaporphines (OAs, Fig. 1) isolated from *Menispermum dauricum* DC roots (family Menispermaceae) [21–23]. *Menispermum dauricum* DC roots as a perennial herb distributed in the northeast, north and east of China, southern Japan, Korea and Russian Siberia widely has been used as traditional medicine treatment for analgesic and antipyretic [24]. OA is a kind of 1-azabenzanthrone derivative with a large planar aromatic conjugated structure that can stabilize the G-quadruplex structure by π–π stacking and electrostatic interactions with G-quartet plane of G-quadruplex DNA [25]. Oxoisoaporphine alkaloids have been reported to have anticancer cells activities through several mechanisms including reactive oxygen species generation, DNA binding [26, 27], and telomerase enzyme inhibition [26, 28, 29]. In addition, OAs also exhibited variety of biological activities including anti-depressant [30], anti-Alzheimer's disease [30–32] and anti-leishmanial activity [33]. Here, we found that the presence of the natural phenalenone skeleton in OAs gave them singlet oxygen photosensitization capacity. However, there are few investigations on their application in PDT. OA has poor water solubility, weak fluorescence and short absorption wavelength, making it unsuitable for PDT. With the goal of developing a novel high-efficiency photosensitizer, here we introduced an electron donating group hydroxyl to OA to enhance the fluorescence quantum yield and water solubility. The generated 4-hydroxyl-oxoisoaporphine (OHOA), as a theranostic agent, has excellent oxygen-generating ability, strong fluorescence and can kill various cancer cells upon irradiation through intrinsic mitochondrial apoptosis.

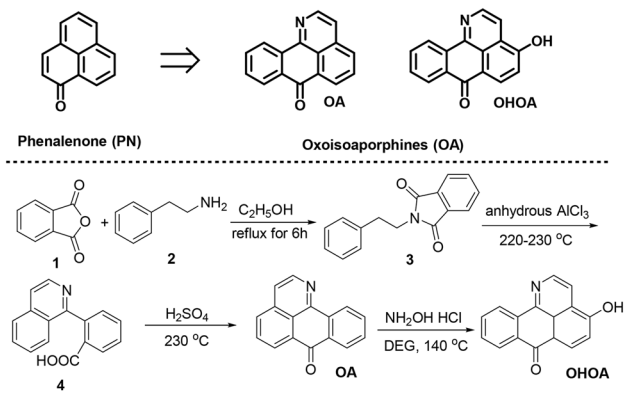

Fig. 1 Synthesis routes for OHOA

2 Materials and methods

2.1 Chemicals and reagents

All chemical reagents or biological reagents and solvents were purchased from commercial suppliers without further purification. ^{1}H NMR and ^{13}C NMR spectra were recorded on Bruker AM-400 (^{1}H at 400 MHz, ^{13}C at 100 MHz) spectrometer with $CDCl_3$ or DMSO-d_6 as the solvent and TMS as the internal standard. High-resolution mass spectra (HRMS) were collected in an XEVO G2 TOF mass spectrometer (Waters, USA) using electrospray ionization (ESI). The optical properties were tested by All Varian Cary 100 UV spectrophotometer and Varian Cary Eclipse FL spectrophotometer.

2.2 Synthesis of phenalenone (PN)

Naphthalene (0.64 g, 5 mmol) and anhydrous aluminum chloride (1.4 g, 5.5 mmol) were put into 10 mL of dichloromethane, stirred for 5 min in an ice bath, cinnamoyl chloride (0.83 g, 5 mmol) was dissolved in 2.5-mL dichloromethane and then dropped into the flask during 30 min, reacted at room temperature for 20 min, the reaction solution was rotary evaporated under vacuum condition purified with silica gel chromatography using petroleum ether/ethyl acetate (10:1) as eluting solvent to afford phenalenone as a yellow solid with a yield of 76% (0.40 g) [34]. ^{1}H NMR (400 MHz, Chloroform-*d*) δ 8.59 (d, $J = 7.6$ Hz, 1H), 8.16

(d, $J = 8.0$ Hz, 1H), 7.98 (d, $J = 8.0$ Hz, 1H), 7.77–7.67 (m, 3H), 7.55 (t, $J = 7.6$ Hz, 1H), 6.71 (d, $J = 9.8$ Hz, 1H). ^{13}C NMR (100 MHz, Chloroform-*d*) δ 185.14, 137.17, 132.90, 132.63, 131.84, 131.61, 131.51, 130.24, 129.30, 129.25, 127.89, 127.15, 126.61. HRMS (ESI): m/z calcd for $C_{13}H_9O^+$ $[M+H]^+$: 181.0653; found: 181.0654.

2.3 Synthesis of oxoisoaporphines (OA)

A mixture of phthalic anhydride (15 g, 100 mmol) and b-phenylethylamine (12.1 g, 100 mmol) in anhydrous ethanol was refluxed for 6 h. After cooling to 0–5 °C, crystals of phenylethylphthalimide (19 g, 78%) separated. Then filtered off to give a solid, washed twice with ethanol. The product is pure enough for the next reaction. To a mixture of anhydrous aluminum chloride (50 g, 0.38 mol) and sodium chloride (9.9 g, 0.17 mol) was slowly added phenylethylphthalimide (25.1 g, 0.1 mol) at 180 °C for 30 min. The reaction was allowed to continue at 220–230 °C for 2 h. The product was cooled, finely ground and poured slowly into concentrated sulfuric acid (550 mL) at 90 °C. The mixture was stirred and heated at 230–240 °C for 2 h. After being cooled, the solution was poured into ice. Sodium hydroxide was added until pH = 3 was obtained and the resultant precipitate was filtered off and washed in turn with dilute aqueous sodium hydroxide and water to give the crude product, which was extracted with acetic acid. The extract was condensed under reduced pressure and the resultant precipitate was washed off, dried, purified with silica gel chromatography using dichloromethane as eluting solvent to afford as a light yellow solid with a yield of 28% (9 g) [35]. ^{1}H NMR (400 MHz, Chloroform-*d*) δ 8.87 (d, $J = 8.0$ Hz, 1H), 8.74 (d, $J = 5.2$ Hz, 1H), 8.62 (d, $J = 7.2$ Hz, 1H), 8.39 (dd, $J = 7.8$, 1.4 Hz, 1H), 8.11 (d, $J = 8.4$ Hz, 1H), 7.88 (t, $J = 7.8$ Hz, 1H), 7.80 (m, 1H), 7.71 (d, $J = 5.6$ Hz, 1H), 7.64 (t, $J = 7.6$ Hz, 1H). ^{13}C NMR (100 MHz, $CDCl_3$) δ 183.31, 148.70, 143.97, 136.69, 135.12, 134.01, 133.35, 132.34, 130.53, 130.38, 129.85, 129.06, 127.55, 125.30, 122.86, 120.89. HRMS (ESI): m/z calcd for $C_{16}H_{10}NO^+$ $[M+H]^+$: 232.0762; found: 232.0761.

2.4 Synthesis of oxoisoaporphines-OH (OHOA)

A mixture of oxoisoaporphines (0.50 g, 2.2 mmol) and hydrazine hydrate (1 mL) was stirred in diethylene glycol (15 mL) for 10 min. Then, 2 mL of 40% NaOH solution was added dropwise, and the mixture was heated at 140 °C for 3 h. The reaction mixture was cooled to room temperature, and poured into water. The hydrochloric acid was added to adjust the solution to pH = 3. The precipitate was filtered off and purified with silica gel chromatography using chloroform/methanol (100:5) as eluting solvent to afford compound 3a as a yellow solid with a yield of 76% (0.40 g) [36]. ^{1}H NMR (400 MHz, DMSO-d_6) δ 12.12 (s, 1H), 8.83 (d, $J = 7.6$ Hz, 1H), 8.77 (d, $J = 5.6$ Hz, 1H), 8.48 (d, $J = 8.4$ Hz, 1H), 8.28 (dd, $J = 7.8$, 1.4 Hz, 1H), 8.10 (d, $J = 5.6$ Hz, 1H), 7.90–7.83 (m, 1H), 7.76–7.70 (m, 1H), 7.33 (d, $J = 8.0$ Hz, 1H). ^{13}C NMR (100 MHz, DMSO-d_6) δ 180.57, 160.44, 146.81, 142.88, 136.00, 133.29, 132.93, 132.20, 130.28, 126.63, 126.14, 124.76, 123.36, 119.65, 116.10, 113.03. HRMS (ESI): m/z calcd for $C_{16}H_{10}NO_2^+$ $[M+H]^+$: 248.0713; found: 248.0712.

2.5 Cell culture and treatment

Human cell lines HeLa (human cervical carcinoma cell) were purchased from the Cell Bank of Type Culture Collection of the Chinese Academy of Sciences (Shanghai, China). The cells were cultured in Dulbecco's modified Eagle's medium (DMEM, Hyclone, Logan, Utah, USA) supplemented with 10% of heat-inactivated fetal bovine serum (FBS, Gibco, Grand Island, NY, USA), 100 U mL^{-1} of penicillin and 100 μg mL^{-1} of streptomycin (Gibco, USA), and then put in a 5% CO_2 atmosphere hatching incubator at 37 °C. The cells were regularly subcultured to maintain them in a logarithmic phase of growth.

2.6 Singlet oxygen detection

To detect the irradiation-induced singlet oxygen ($^1O_2$), a singlet oxygen trap 9,10-anthracenediylbis (methylene) dimalonic acid (ABDA) was used in air-saturated MilliQ water to monitor the $^1O_2$ generation. Water-soluble ABDA exhibits photobleaching when oxidized by singlet oxygen to endoperoxide, which causes the degradation of ABDA at 400 nm. Compounds were dissolved in MilliQ water (0.5% DMSO as cosolvent) and then added to equivalent ABDA stock solution. After light (470 nm, 5 mW cm^{-2}) irradiation, the absorbance of ABDA at 400 nm was recorded every 5 min. Phenalenones was utilized as a control. The control experiment was carried out using 10 mM ABDA without photosensitizer. The decomposition of ABDA by OA, OHOA and PN with different irradiation time in water is compared in Fig. 2c. A_0 is the absorbance of ABDA at 400 nm before irradiation, A is the absorbance of ABDA at 400 nm under different irradiation time. The direct evidence of $^1O_2$ could be obtained by EPR technique [37–40], the experimental data were shown in supporting information. Photostability experiment was carried out as following description: samples dissolved in MilliQ water (10^{-5} M, 0.5% DMSO as cosolvent) was irradiated with a LED light (460–470 nm, 5 mW cm^{-2}) for 3 h, then absorbances were collected every 30 min during irradiation. The changes of optical density at λ_{max} with irradiation time under blue light were recorded in Fig. 2c. During irradiation, the samples were stirred and the temperature was kept constant. Singlet

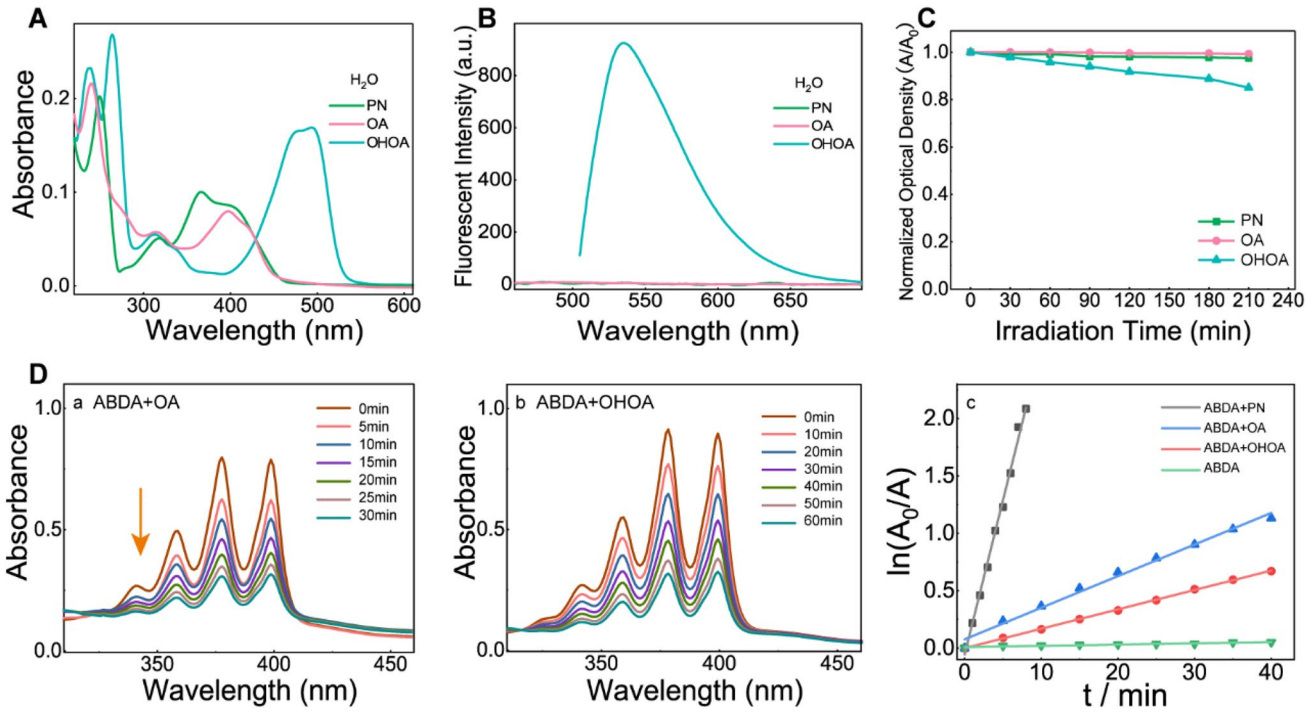

Fig. 2 **a** UV–Vis absorption spectra and **b** fluorescent emission spectra of targeted compounds in H_2O ($\lambda_{ex}=490$ nm, $\lambda_{em}=528$ nm). **c** Absorption spectrum changes of compounds after irradiation with blue light (5 mW cm^{-2}) for different periods of time. A_0 is the absorbance at the maximum absorption wavelength before irradiation, A is the absorbance at the maximum absorption wavelength after different irradiation durations. **d** The changes of absorbance at 400 nm of ABDA as a function of irradiation time

oxygen quantum yields of test compounds were obtained based on following equation:

$$\phi_{\Delta}(\mathrm{PS}) = \phi_{\Delta}(\mathrm{ST})\frac{k_{\mathrm{PS}}}{k_{\mathrm{ST}}}.$$

When ϕ_{Δ} means the singlet oxygen quantum yields of photosensitizer and PN as a reference ($\phi_{\Delta}=1$ in water), k is the plot of the logarithm of change in ABDA absorbance at 400 nm versus irradiation time.

2.7 Fluorescence quantum yield calculation

OHOA was formulated with MilliQ water (5% DMSO as cosolvent) to 10^{-5}–10^{-6} M, the absorbance spectra were collected on Varian Cary 100 UV–Vis spectrophotometer and the corresponding fluorescence spectra were obtained on a Varian Cary Eclipse Fluorescence spectrophotometer. The fluorescent quantum yields of test compounds were obtained based on following equation:

$$\phi_{F}(\mathrm{PS}) = \phi_{F}(\mathrm{ST})\frac{\mathrm{Grad}_{\mathrm{PS}}}{\mathrm{Grad}_{\mathrm{ST}}}\frac{\eta_{\mathrm{PS}}^2}{\eta_{\mathrm{ST}}^2}.$$

When ϕ_F means the fluorescent quantum yields of photosensitizer and naphthalimide as a reference ($\phi_F(\mathrm{ST})=0.66$ in ethanol), Grad is the gradient form the plot of integrated fluorescence intensity versus absorbance, η is the refractive index of the solvent.

2.8 Photoinduced cytotoxicity test

PDT efficacy of OHOA was determined by MTT assay using HeLa cancer cell lines. PDT utilizes $^1O_2$ generated by photosensitizers when absorb specific wavelengths of light, causing oxidative stress on tissues and abnormal proliferation of active cells. In this respect, PDT is applicable to all kinds of tumor cancer cells. We choose three other cancer cells besides HeLa cells including A549 (human lung adenocarcinoma cell), HepG2 (human hepatocellular carcinomas cell) and MCF7 (human breast cancer cells). The cytotoxicity of OAs were evaluated towards different cancer cells in the light stimulation and dark condition and the half maximal inhibitory concentration (IC_{50}) values against different cell lines were summarized in supplementary information. Cells were digested with trypsin to make a single cell suspension (1×10^5 cells mL^{-1}) and were seeded onto 96-well plates (100 µL per well) for 12 h. Two 96-well plates were set as control trails. One plate was accepted with light stimulation, while the other one was kept in dark condition. Compounds were formulated with culture medium to different concentration including 0.1% DMSO as cosolvent. After removing the

original culture medium, chemicals of series of concentrations (200 μL per well) was added to 96-well plates. After 24 h incubation in darkness, the samples were subjected to a 470–480 nm LED light at power density of 20 mW cm^{-2} for 20 min (fluence, 40 J cm^{-2}). After 24 h incubation, 20 μL of MTT (5 mg mL^{-1}) was added to each well. After 4 h incubation at 37 °C, culture medium was discarded and the residue was added 150 μL DMSO to dissolve the purple formazan crystals. Absorbance was measured at 570 nm and 630 nm by a Synergy H1 microplate reader (Bio-Teck, Winooski, VT, USA). The inhibitory rates of the cells were calculated by the following formula:

$$\%\ \text{inhibitory rate} = \left\{ 1 - \frac{\text{mean}\left[\text{OD}_{570\text{nm}}(\text{sample}) - \text{OD}_{630\text{nm}}(\text{sample})\right]}{\text{mean}\left[\text{OD}_{570\text{nm}}(\text{control}) - \text{OD}_{630\text{nm}}(\text{control})\right]} \right\} \times 100\%,$$

where OD (sample) and OD (control) were denoted as the absorbance of the sample solution and control wells, respectively. The MTT assay was performed in triplicate, the mean and standard deviation was calculated for each group.

2.9 Clonogenic assay

The effectiveness cytotoxicity of OHOA with or without light irradiation was compared by employing clonogenic assay. Clonogenic assay is an in vitro cell survival assay to determine the ability of a single cell to grow into a colony. Here, a colony is defined as a cluster of at least 50 cells. Cells were seeded in 6 cm dish at a density of 1×10^3 cells mL^{-1} and cultivated in incubator for 12 h. The medium in the dish (4 mL) was then replaced with fresh medium containing OHOA (10 μM) and the light group was subjected to light stimulation, then the cells were incubated continued for 2 weeks with culture medium that was refreshed every 2 days. Colonies were rinsed with PBS, fixed with 4% paraformaldehyde for 1 h at room temperature and stained with 10% Giemsa staining solution for 1 h. After cells were washed with PBS and air-dried, colonies consisting of more than 50 cells were counted. Each experiment was done in triplicate and colony number in the absence of OHOA was used as a control. Six experiments groups (dark control, light control, OHOA in dark, OHOA plus with 5-min light irradiation, OHOA plus with 15-min light irradiation and OHOA plus with 30-min light irradiation) were conducted simultaneously.

2.10 Localization of OHOA by fluorescence observation

Cellular uptake and intracellular imaging efficiency were performed by confocal laser scanning microscope on Human Cervical Cancer cell line, HeLa cells, as model system. HeLa cells (1×10^5 cells mL^{-1}) were seeded on a glass bottom cell culture dish and co-incubated with OHOA (2.5 μM) for 6 h. After 15 min of PDT treatment, to explore the subcellular localization of OHOA, one dish of cells was washed with PBS for three times and incubated in culture medium with 100 nm MitoTracker Red (invitrogen™) for 20 min, another dish of cells was incubated with 50 nm Lysosome Tracker Red (invitrogen™) for 30 min. Then, stained live cells were observed by confocal laser scanning microscope (Nikon Inc., Melville, NY, USA). Emission was collected at 530 ± 20 nm upon excitation at 488 nm for OHOA. MitoTracker Red and Lysosome Tracker Red were excited at 561 nm and emissions were collected at 599 ± 20 nm.

2.11 Intracellular ROS detection by confocal microscope

2′,7′-Dichlorofluorescin diacetate (DCFH-DA) (Sigma-Aldrich, USA) was selected to detect the intracellular ROS. HeLa cells (5×10^5 cell mL^{-1}) were seeded to glass bottom cell culture dish for overnight, then treated with different concentrations (dark control, light control, OHOA in dark, OHOA plus with light irradiation for 5 min, OHOA plus with light irradiation for 15 min, OHOA plus with light irradiation for 30 min). After that, cells were incubated with 10 μM H_2DCFDA for 20 min. Then, cells were washed three times with PBS, analyzed immediately by confocal laser scanning microscope (Nikon Inc., Melville, NY, USA). Emission was collected at 530 ± 20 nm upon excitation at 488 nm. Flow cytometric analysis was utilized to detect intracellular reactive oxygen quantitatively. HeLa cells (10^6 cell mL^{-1}) were seeded in a 6-well culture plates and were treated with different conditions as described before, then digested and collected in 1.5-mL centrifuge tube, washed with PBS for three times (1500 rpm). H_2DCFDA (10 μM final concentration) was added to the cell and then incubated at 37 °C for 20 min. Cells were washed with PBS for three times before they were analyzed on a FAC Scan flow cytometer (BD, FACS Calibur). The fluorescence intensity of cells was measured with excitation 488 nm and emission at 530 nm. Green mean fluorescence intensities were analyzed using FlowJo 7.6 software.

2.12 Mitochondrial membrane potential (△Ψm) analysis

JC-1 can easily penetrates cells and healthy mitochondria. In normal mitochondria with high membrane potential JC-1

keeps aggregated and the fluorescence is red, while in dysfunctional mitochondria with decreased membrane potential, JC-1 keeps monomeric and fluoresces green. Therefore, the red/green fluorescence ratio represented the status of mitochondria to some extent. HeLa cells (5×10^5 cell mL^{-1}) were seeded to glass bottom cell culture dishes for overnight, then treated with different conditions as described before. After treatment, the cells were incubated at 37 °C for 30 min with 5 mg L^{-1} JC-1 (Invitrogen™), washed twice with PBS and placed in fresh medium without serum. Finally, images were viewed and scanned by confocal laser scanning microscope (Nikon Inc., Melville, NY, USA) at 488 nm excitation and emission at 530 nm for green, and at 561 nm excitation and emission at 590 nm for red. Confocal images of JC-1 staining were processed as red/green signal ratio, relative intensity was calculated using ImageJ software. Mitochondrial depolarization was indicated by an increase in the ratio of green/red fluorescence intensity.

2.13 Chromatin morphology assay

Cells were treated as described before. Hoechst 33342 nuclear staining procedure was chosen to observe the changes of cells morphology which were induced by OHOA. After the HeLa cells were treated with different conditions, cells were washed three times with serum-free medium, then fixed with paraformaldehyde under 4 °C for 15 min, wash twice with PBS, and incubated with Hoechst 33342 (10 μM) at 37 °C for 10 min, after that washed three times with PBS (pH 7.4). The morphology of Hela cells was observed and photographed by confocal laser scanning microscope (Nikon Inc., Melville, NY, USA). Emission was collected at 460 ± 20 nm upon excitation at 346 nm for blue, at 488 nm excitation and emission at 530 nm for green.

2.14 Apoptosis analysis by Annexin V-FITC/PI apoptosis kit

To explore the apoptosis-induced effects of OHOA, the percentage of apoptotic cells by flow cytometry with Annexin V-FITC/PI apoptosis kit (Invitrogen™) were analyzed. In brief, HeLa cells cultured in 6-well plates were treated with various conditions (OHOA in dark, OHOA with light irradiation for 5 min, OHOA with light irradiation for 15 min, OHOA with light irradiation for 30 min) for 2 h, 1×10^6 cells were washed, trypsinized and collected in 1.5-mL centrifuge tube. Then, the cells were washed with PBS (pH 7.6) for three times (2000 rpm). After centrifugation, the cells collected and resuspended in 500 μL of buffer solutions loaded with Annexin V-FITC and PI (with 5 μL Annexin V-FITC and 10 μL PI) for 15 min. Finally, the Annexin V-FITC-stained cells were tested on flow cytometer (BD, FACS Calibur) and the data were analyzed using FlowJo 7.6 software.

2.15 Western blotting analysis

Total protein from HeLa cells was extracted in RIPA lysis buffer (Sigma-Aldrich, St. Louis, MO, USA) with 1 mM phenylmethylsulfonyl fluoride (PMSF, Sigma-Aldrich, St. Louis, MO, USA), and quantified by BCA method. Cellular extracts were separated on 10–15% SDS-PAGE and transferred to a polyvinylidene difluoride (PVDF) membrane (Millipore Corp, Atlanta, GA, USA) from gel. Then blocked in Tris-buffered saline-Tween (TBST; 10 mM Tris–HCl, pH 7.5/150 mM NaCl/0.1% Tween-20) with 5% non-fat dry milk for 1 h at room temperature. These was then incubated with antibodies for caspase 3 (1:1000), cleaved-caspase 3 (1:1000), PARP (1:1000) and β-actin (1:1000) overnight at 4 °C, subsequently incubated with HRP conjugated secondary antibodies for 2 h at room temperature. Signals were visualized after treatment by enhanced chemiluminescence (ECL) reagent (Pierce, Rockford, IL, USA). All protein bands were scanned.

2.16 Statistical analysis

All experiments were performed in triplicate and repeated at least three times. Data were shown as means ± standard deviations (SDs). The results were analyzed by one-way analysis of variance (ANOVA) followed by post hoc statistical tests, using the Tukey test for each pair of compared groups. Statistical significance was defined as $*p<0.05$, $**p<0.01$, $***p<0.001$.

3 Results and discussion

3.1 Synthesis

The synthetic routes of oxoisoaporphine derivative was depicted in Fig. 1. OA and OHOA were synthesized by a four-step reaction. *O*-phthalic anhydride **1** reacted with amine **2** gave phthalimide **3**. Treatment of **3** with anhydrous aluminum chloride at 220–230 °C provided intermediate **4**. Finally, intermediate **4** reacted with sulfuric acid affording the target compound OHOA. Reaction of OA with hydroxylamine hydrochloride at 140 °C offered the target compound OHOA.

3.2 Photophysiochemical properties

To determine the performance of OA and OHOA, their photophysiochemical properties, such as maximum absorption and emission wavelength, and photostability and singlet oxygen-generating ability were investigated. OA has two absorption bands in acetonitrile centered at 250 nm and 390 nm, respectively. The molar extinction coefficients of

OA and OHOA are 11,012 M^{-1} cm^{-1} and 14,997 M^{-1} cm^{-1}, respectively. In PBS buffer, a bathochromic shift occurred for OHOA with the appearance of a new absorption band around 490 nm (Fig. 2a). This can be attributed to deprotonization of the hydroxyl group. A high fluorescence quantum yield facilitates cell imaging and diagnosis for a photosensitizer. OA was weakly emissive, while OHOA showed strong fluorescence emission with quantum yields approaching 0.72 (PBS buffer, naphthalimide as reference, $\Phi_F = 0.66$ in ethanol) and an emission maximum wavelength occurring at around 535 nm (Fig. 2b). 9,10-Anthracenediylbis (methylene) dimalonic acid (ABDA) was used to detect the ability of singlet oxygen generation by OAs in water under irradiation. The reaction of ABDA and singlet oxygen cause the decrease of ABDA absorbance at a wavelength of 400 nm. Figure 2d shows linear relationship between irradiation time and the logarithm of change in ABDA absorbance at 400 nm. Phenalenone produced singlet oxygen at a faster rate than OA and OHOA. The photodegradation processes of PN, OA and OHOA were monitored by optical density changes at λ_{max} upon blue light (470 nm, 5 mW cm^{-2}) irradiation. No obvious photodegradation was detected when OA and OHOA were subjected to irradiation at 470 nm for 3 h in PBS buffer (Fig. 2c), this demonstrated their stability during of biological testing and in the presence of light.

3.3 Phototoxicity evaluation

The cytotoxicity of OAs towards HeLa cells was evaluated in light stimulation and dark conditions. A summary of half maximal inhibitory concentration (IC_{50}) values is shown in Fig. 3a. In general, all compounds exhibited higher toxicity upon irradiation in comparison with dark conditions, indicating that OA and OHOA have obvious photo-dependent activity towards HeLa cells. OA has moderate dark toxicity to HeLa cells with IC_{50} values of 41.04 μM, which corresponds well to previously reported results. When exposed to light, cytotoxicity increased by tenfold for OA. OHOA exhibited significant activity enhancement after light irradiation, with an increase in cytotoxicity of about 150-fold. The lack of cytotoxicity in dark verified that OHOA is safe for normal tissues in PDT treatment. The degree of light irradiation on the anticancer effects of OHOA is shown in Fig. 3b. The increasing cytotoxicity correlated closely with the increasing duration of light irradiation, as the viability of HeLa cells decreased from 43.88 to 8.23%. Similar results were also observed in colony growth. When the irradiation time increased from 5 to 30 min, colony growth decreased by 57.75%, 85.56% and 97.69%, respectively (Fig. 3c), in comparison with the dark control.

3.4 Intracellular singlet oxygen detection

After the photosensitizer is absorbed by cells, large amount of reactive oxygen species (ROS) including singlet oxygen produced rapidly after illumination, which caused the imbalance of intracellular reactive oxygen species and oxidation stress [41]. To identify the light-induced mechanism behind the light-responsive toxicity, 2′,7′-dichlorofluorescin diacetate (DCFH-DA) was used as an indicator to detect ROS produced in HeLa cells. The HeLa cells were subjected to six different conditions: no treatment (negative control), light treatment only, OHOA in dark, and OHOA plus different irradiation times (5, 15 or 30 min). Fluorescence microscopy images were collected at 530 nm upon excitation at 488 nm. For HeLa cells treated with OHOA and light (470 nm, 20 mW cm^{-2}), a significant fluorescence increase was observed (Fig. 4a). When OHOA was irradiated for 5 min, the mean fluorescence intensity quickly rose to 101, which is approximately double that of OHOA in dark conditions. Similar results also were obtained by flow cytometric analysis (Fig. 4b). These findings suggest that OHOA treatment together with light can efficiently produce high cytotoxic ROS levels in HeLa cells.

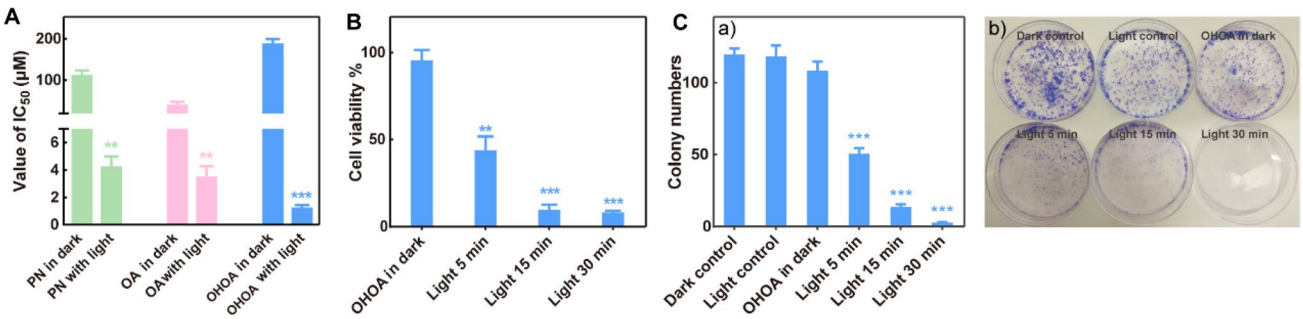

Fig. 3 **a** In vitro dark toxicity and phototoxicity of IC_{50} values for PN, OA and OHOA in HeLa cells at 48 h post-treatment. **b** Effects of light dose on HeLa cells viability, OA2 concentration: 10 μM. **c-a** Colony numbers counted using Image J. **b** Digital images of clonogenic assay performed in six-well plates, with clones produced by HeLa cells under different conditions. All the data are presented as mean ± SD ($n = 3$ per group). Significant differences from dark control: *$p < 0.05$; **$p < 0.01$; ***$p < 0.001$

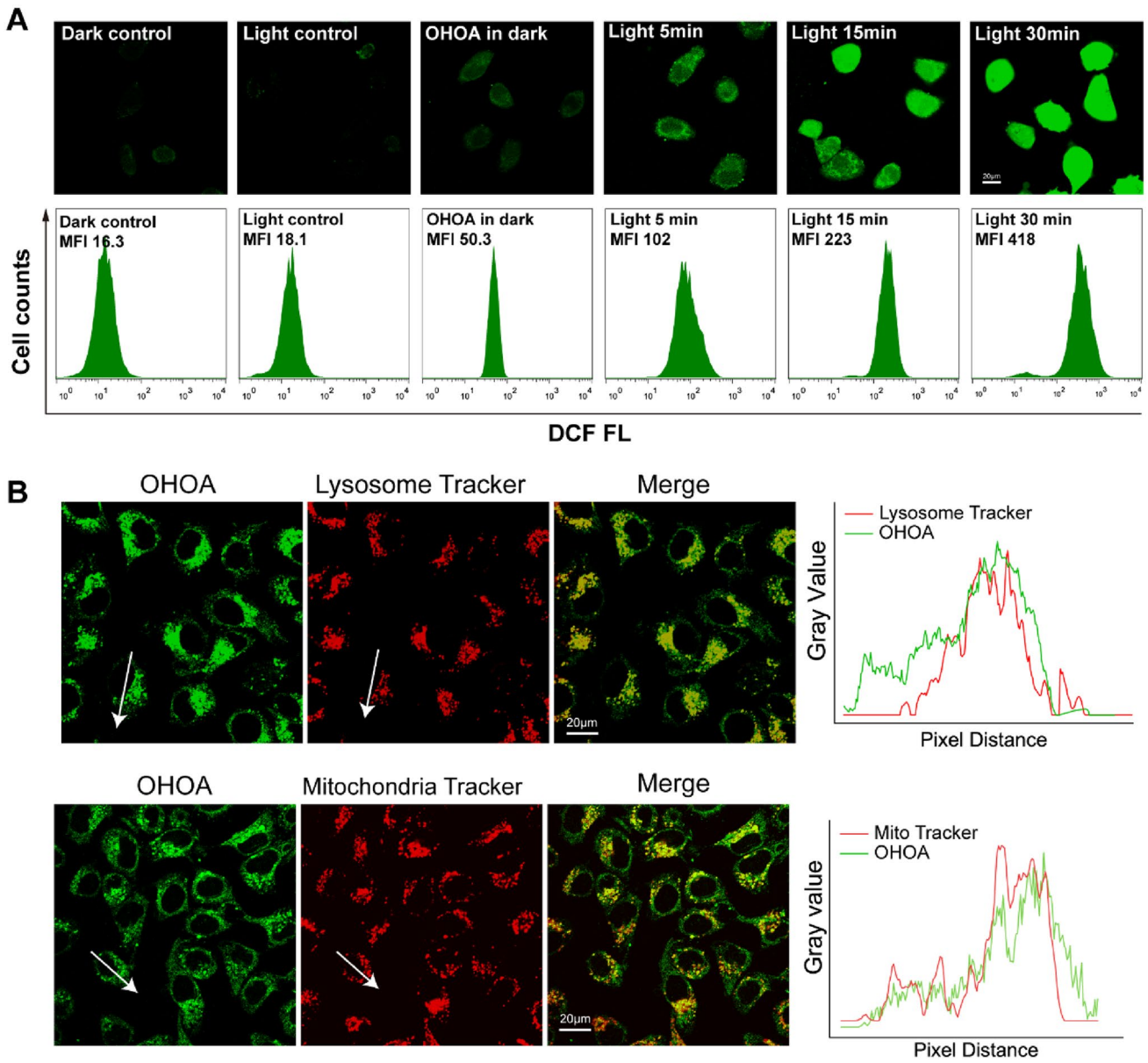

Fig. 4 **a** Confocal microscopic images and flow cytometric quantification of cellular ROS levels detected by DCFH-DA staining. Scale bar: 20 μM. *MFI* mean fluorescence intensity. **b** Confocal microscopy images of HeLa cells incubated with OHOA (2.5 μM) and treated with commercial organelle trackers. Overlay images and colocalization analysis of cells stained with mitochondria (Pearson coefficient = 0.52), and lysosome (Pearson coefficient = 0.54). Scale bar: 20 μM. The representative fluorescence line profiles of the white arrows show colocalization efficiencies

3.5 Subcellular localization

Since the OHOA has high fluorescence quantum yield, the intracellular imaging efficiency of OHOA during therapy on HeLa cells was studied via confocal laser scanning microscopy. OHOA could easily pass through the cell membrane and visualize cells morphology before or after treatment. Images indicated that OHOA predominantly distributed in the cytoplasm rather than in the nucleus. Subsequently, to explore the subcellular localization of OHOA in cells, fluorescent localization probes of mitochondria and lysosome were applied for colocalization inside cells (Fig. 4b). The merged images demonstrated that OHOA mainly accumulated in the lysosome with a Pearson coefficient of 0.54 and in mitochondria with a Pearson coefficient of 0.52. These phenomena indicated that OHOA could optimize the imaging results for monitoring therapy processes to ensure anticancer therapeutic effects.

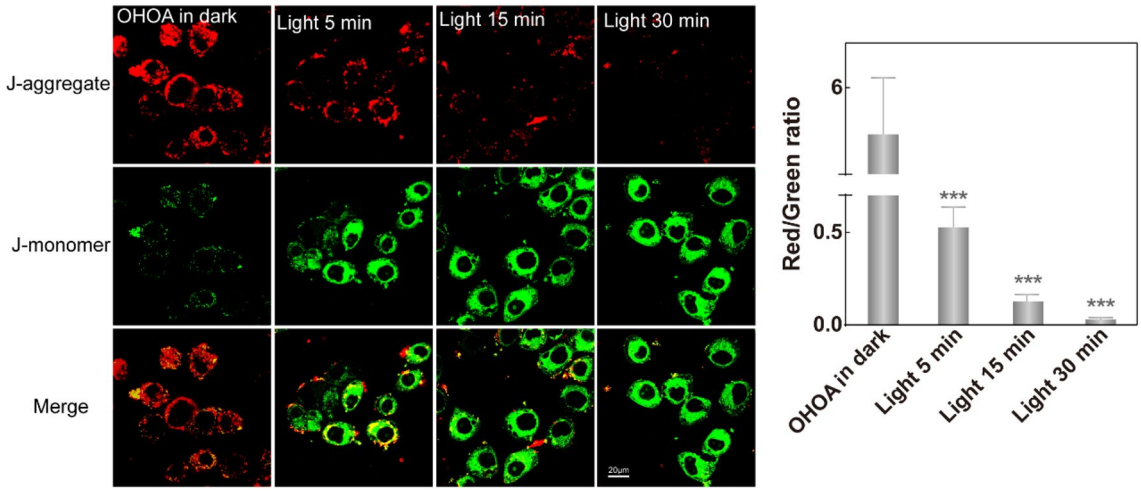

Fig. 5 **a** Effects of OHOA in dark or irradiated with blue light on the $\Delta_{\Psi m}$ of Hela cells. Cells were treated with OHOA under various conditions (OHOA in dark, OHOA with 5/15/30 min light irradiation). Scale bar: 20 μM. **b** Quantitative fluorescence analysis of JC-1 (red/green ratio). Data are expressed as mean ± SD of three separate sets of independent experiments. Significant differences from OHOA in dark: $^{*}p < 0.05$; $^{**}p < 0.01$; $^{***}p < 0.001$

3.6 OHOA induces cell apoptosis

Furthermore, on the basis of mitochondrial location behavior of fluorescence confocal imaging, a series of trials were designed and conducted on HeLa cells to confirm the detection of OHOA-PDT-induced cell apoptosis. Generation of singlet oxygen in mitochondria can trigger a rapid apoptotic response in cell. Mitochondrial membrane potential is a marker of mitochondrial disorder associated closely with apoptosis. We chose JC-1 dye as the sensor to detect mitochondrial membrane potential of HeLa cells incubated with OHOA under different conditions. Red fluorescence appeared when no irradiation was performed (Fig. 5a). Green fluorescence became stronger and stronger when irradiation time was increased from 5 to 15 min. The ratio of red/green fluorescence intensity representing mitochondrial membranes decreased from 5.46 (OHOA in dark) to 0.03 (irradiation with light for 30 min), as shown in Fig. 5b. This observation indicates that light can trigger the generation of ROS in mitochondria in situ. ROS damaged mitochondria and led to a significant decrease in membrane potential.

To further determine the cell apoptosis mechanism of OHOA in the PDT process, we investigated the expression

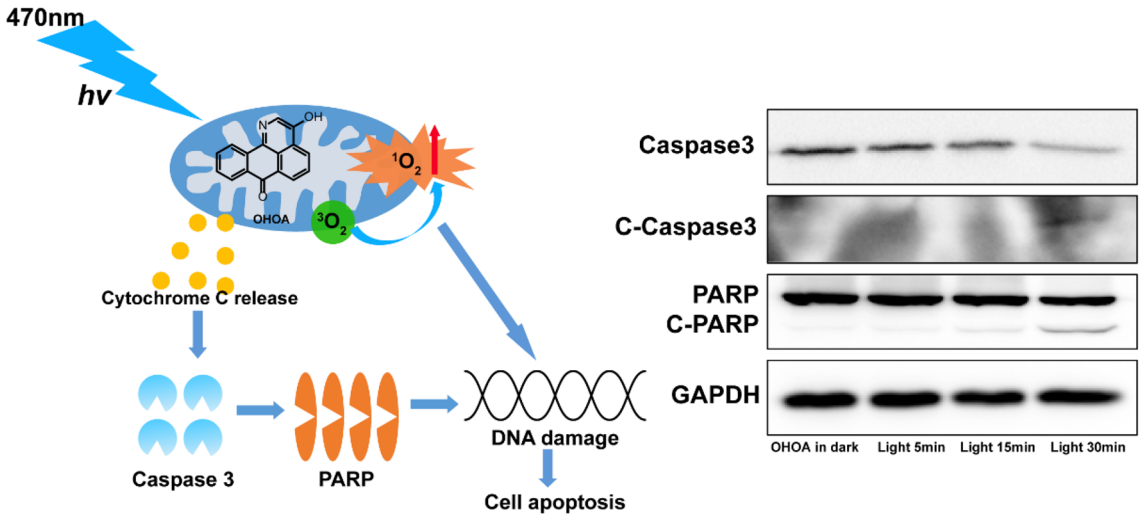

Fig. 6 Western blot assays of OHOA-PDT on expression of caspase 3 and cleaved-caspase 3, PARP, cleaved-PARP. GAPDH was determined as an internal reference protein

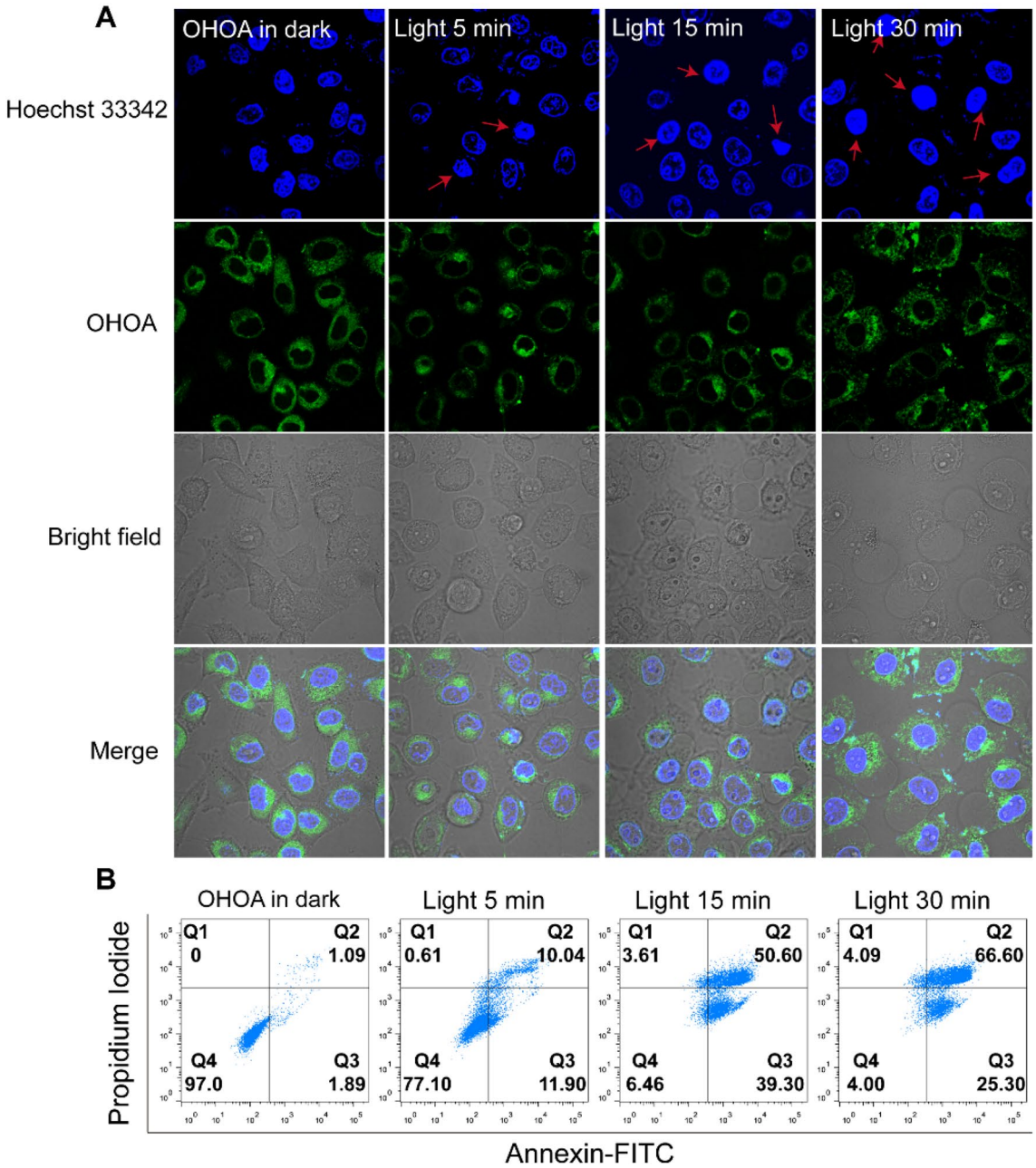

Fig. 7 **a** DNA fragmentation and chromatin condensation were observed under different conditions. OHOA-PDT-induced HeLa cell apoptosis in a light dose-dependent manner. **b** OHOA with light-induced apoptosis of HeLa cells analyzed by flow cytometry after Annexin V-FITC and PI staining

levels of the caspase family, which plays a key role in the apoptotic process. The protein levels in the apoptotic pathway, caspase 3 and PARP (poly ADP-ribose polymerase) were assayed for the OHOA- and light-treated HeLa cells. After receiving an apoptotic $^1O_2$ stimulus generated in the intracellular matrix or mitochondria, cytochrome c is released from the intermembrane space of the mitochondria into the cytoplasm. Then, cytochrome c in the cytoplasm executes a series of functions to recruit and facilitate downstream activation of caspase 3, which subsequently leads to the cleavage of PARP and triggered the caspase-3-dependent apoptotic pathway. The cleaved-caspase 3 and cleaved-PARP were increased in an irradiation time-dependent manner (Fig. 6).

ROS overproduction can induce DNA destruction in the nuclei of cancer cells [42], we subsequently selected Hoechst 33342 nuclear staining to observe the changes in cell morphologies induced by OHOA. Morphologies

of HeLa cells were imaged by fluorescence microscope (Fig. 7a). The chromatin fluorescence of OHOA treated cells in dark conditions stained dimly and was observed in the majority of the cells, indicating that OHOA treatment without illumination did not cause any damage to HeLa cells. HeLa cells incubated with OHOA and light stimulation underwent significant chromatin condensation, shrinkage, formed bubbles and DNA fragmentation. In addition, the chromatin fluorescence intensity was notably enhanced. This phenomenon indicated that ROS generated in the intracellular matrix by OHOA-PDT increased the level of DNA damage. To explore the light-induced apoptosis effects of OHOA, the percentage of apoptotic cells was analyzed by flow cytometry using an Annexin V–FITC/PI apoptosis kit (Invitrogen™). In flow cytometry assays, Annexin V–FITC–/PI– (viable cells), Annexin V–FITC+/PI– (early apoptotic cells), and Annexin V–FITC+/PI+ (necrotic or late-stage apoptotic cells) were used to determine cell populations at different stages of cell death. A high efficiency of OHOA-mediated PDT was observed. An increased proportion of the apoptotic cells were observed following prolonged irradiation times (Fig. 7b). When the irradiation time is extended from 5 to 15 min, the proportion of apoptotic cells increased from 22.30 to 91.90%.

4 Conclusions

In summary, we synthesized and characterized a phenalenone-based photosensitizer (OHOA). OHOAs have improved water solubility and relatively longer absorption wavelengths in comparison with phenalenone precursors. Oxoisoaporphines display a PS-like activity due to a phenalenone (PN) moiety—an efficient singlet oxygen photosensitizer—in its skeleton. Compared to PN, OHOA has lower singlet oxygen generation quantum yields but higher photo-cytotoxicity partly due to the localization in subcellular organelle. Most importantly, OHOA has high fluorescence quantum yield (0.72), making it possible to work as a potential photodynamic therapeutic and theranostic agent simultaneously. When stimulated by light, OHOA blocked cell proliferation and clonogenic potential of cancer cells. In the OHOA-based PDT process, cell apoptosis occurred via the mitochondrial pathway and decreased mitochondrial transmembrane potential was observed. Subcellular-targeting is an attractive strategy to maximize the efficacy of PDT and small molecules such as OHOA with fluorescence can be a very efficient therapeutic and theranostic tool for medical applications.

Supplementary Information The online version contains supplementary material available at https://doi.org/10.1007/s43630-021-00030-0.

Acknowledgements This work was financial supported by National Key Research and Development Program of China (2018YFD0200100), National Natural Science Foundation of China (No. 21877039), Science and Technology Commission of Shanghai Municipality (16391902300) and Innovation Program of Shanghai Municipal Education Commission (2017-01-07-00-02-E00037).

Author contributions XS designed experiments; QX and YJ carried out experiments; MC analyzed experimental results. QX and XS wrote the manuscript.

Data availability All data generated or used during the study appear in the submitted article and supplementary information. The data used to support the findings of this study are also available from the corresponding author upon request.

Declarations

Conflict of interest The authors declare that they have no conflict of interest.

References

1. Lan, M., Zhao, S., Liu, W., Lee, C.-S., Zhang, W., et al. (2019). Photosensitizers for photodynamic therapy. *Advanced Healthcare Materials, 8,* 1900132.
2. Qin, Y., Chen, L.-J., Dong, F., Jiang, S.-T., Yin, G.-Q., et al. (2019). Light-controlled generation of singlet oxygen within a discrete dual-stage metallacycle for cancer therapy. *Journal of the American Chemical Society, 141,* 8943–8950.
3. dos Santos, A. F., de Almeida, D. R. Q., Terra, L. F., Baptista, M. S., & Labriola, L. (2019). Photodynamic therapy in cancer treatment - an update review. *Journal of Cancer Metastasis and Treatment, 5,* 25.
4. Yu, G., Zhu, B., Shao, L., Zhou, J., Saha, M. L., et al. (2019). Host−guest complexation-mediated codelivery of anticancer drug and photosensitizer for cancer photochemotherapy. *Proceedings of the National Academy of Sciences, 116,* 6618.
5. Roy, I., Bobbala, S., Young, R. M., Beldjoudi, Y., Nguyen, M. T., et al. (2019). A supramolecular approach for modulated photoprotection, lysosomal delivery, and photodynamic activity of a photosensitizer. *Journal of the American Chemical Society, 141,* 12296–12304.
6. Yang, J., Cao, Q., Hu, W.-L., Ye, R.-R., He, L., et al. (2017). Theranostic tempo-functionalized Ru(II) complexes as photosensitizers and oxidative stress indicators. *Dalton Transactions, 46,* 445–454.
7. Karges, J., Heinemann, F., Maschietto, F., Patra, M., Blacque, O., et al. (2019). A Ru(II) polypyridyl complex bearing aldehyde functions as a versatile synthetic precursor for long-wavelength absorbing photodynamic therapy photosensitizers. *Bioorganic and Medicinal Chemistry, 27,* 2666–2675.
8. Skovsen, E., Snyder, J. W., Lambert, J. D. C., & Ogilby, P. R. (2005). Lifetime and diffusion of singlet oxygen in a cell. *The Journal of Physical Chemistry B, 109,* 8570–8573.
9. Li, C., Wang, Y., Lu, Y., Guo, J., Zhu, C., et al. (2020). An iridium(III)-palladium(II) metal-organic cage for efficient mitochondria-targeted photodynamic therapy. *Chinese Chemical Letters, 31,* 1183–1187.
10. He, Z., Zhang, Y., Khan, A. R., Ji, J., Yu, A., et al. (2020). A novel progress of drug delivery system for organelle targeting in tumour cells. *Journal of Drug Targeting, 29,* 12–28.

11. Lv, W., Zhang, Z., Zhang, K. Y., Yang, H., Liu, S., et al. (2016). A mitochondria-targeted photosensitizer showing improved photodynamic therapy effects under hypoxia. *Angewandte Chemie International Edition, 55,* 9947–9951.
12. Jana, B., Thomas, A. P., Kim, S., Lee, I. S., Choi, H., et al. (2020). Self-assembly of mitochondria-targeted photosensitizer to increase photostability and photodynamic therapeutic efficacy in hypoxia. *Chemistry-A European Journal, 26,* 10695–10701.
13. Sainuddin, T., McCain, J., Pinto, M., Yin, H., Gibson, J., et al. (2016). Organometallic Ru(II) photosensitizers derived from π-expansive cyclometalating ligands: surprising theranostic PDT effects. *Inorganic Chemistry, 55,* 83–95.
14. Binns, T. C., Ayala, A. X., Grimm, J. B., Tkachuk, A. N., Castillon, G. A., et al. (2020). Rational design of bioavailable photosensitizers for manipulation and imaging of biological systems. *Cell Chemical Biology, 27,* 1063-1072.e7.
15. Lovell, J. F., Liu, T. W. B., Chen, J., & Zheng, G. (2010). Activatable photosensitizers for imaging and therapy. *Chemical Reviews, 110,* 2839–2857.
16. Espinoza, C., Trigos, Á., & Medina, M. E. (2016). Theoretical study on the photosensitizer mechanism of phenalenone in aqueous and lipid media. *The Journal of Physical Chemistry A, 120,* 6103–6110.
17. Flors, C., & Nonell, S. (2006). Light and singlet oxygen in plant defense against pathogens: phototoxic phenalenone phytoalexins. *Accounts of Chemical Research, 39,* 293–300.
18. Hölscher, D., Dhakshinamoorthy, S., Alexandrov, T., Becker, M., Bretschneider, T., et al. (2014). Phenalenone-type phytoalexins mediate resistance of banana plants (*Musa* spp.) to the burrowing nematode *Radopholus similis*. *Proceedings of the National Academy of Sciences, 111,* 105.
19. Späth, A., Leibl, C., Cieplik, F., Lehner, K., Regensburger, J., et al. (2014). Improving photodynamic inactivation of bacteria in dentistry: highly effective and fast killing of oral key pathogens with novel tooth-colored type-II photosensitizers. *Journal of Medicinal Chemistry, 57,* 5157–5168.
20. Song, R., Feng, Y., Wang, D., Xu, Z., Li, Z., et al. (2017). Phytoalexin phenalenone derivatives inactivate mosquito larvae and root-knot nematode as type-ii photosensitizer. *Scientific Reports, 7,* 42058.
21. Sobarzo-Sánchez, E., Soto, P. G., Valdés Rivera, C., Sánchez, G., & Hidalgo, M. E. J. M. (2012). Applied biological and physicochemical activity of isoquinoline alkaloids: oxoisoaporphine and boldine. *Molecules, 17,* 10958–10970.
22. Zhang, X., Ye, W., Zhao, S., & Che, C.-T. (2004). Isoquinoline and isoindole alkaloids from *Menispermum dauricum*. *Phytochemistry, 65,* 929–932.
23. Wei, J., Chen, J., Liang, X., & Guo, X. (2016). Microwave-assisted extraction in combination with HPLC-UV for quantitative analysis of six bioactive oxoisoaporphine alkaloids in *Menispermum dauricum* DC. *Biomedical Chromatography., 30,* 241–248.
24. Zhang, J., Chen, L., & Sun, J. (2018). Oxoisoaporphine alkaloids: prospective anti-Alzheimer's disease, anticancer, and antidepressant agents. *ChemMedChem, 13,* 1262–1274.
25. Chen, Z.-F., Qin, Q.-P., Qin, J.-L., Liu, Y.-C., Huang, K.-B., et al. (2015). Stabilization of G-quadruplex DNA, inhibition of telomerase activity, and tumor cell apoptosis by organoplatinum(II) complexes with oxoisoaporphine. *Journal of Medicinal Chemistry, 58,* 2159–2179.
26. Rodríguez-Arce, E., Cancino, P., Arias-Calderón, M., Silva-Matus, P., & Saldías, M. J. M. (2020). Oxoisoaporphines and aporphines: versatile molecules with anticancer effects. *Molecules, 25,* 108.
27. Qin, J.-L., Qin, Q.-P., Wei, Z.-Z., Yu, Y.-C., Meng, T., et al. (2016). Stabilization of c-myc G-Quadruplex DNA, inhibition of telomerase activity, disruption of mitochondrial functions and tumor cell apoptosis by platinum(II) complex with 9-amino-oxoisoaporphine. *European Journal of Medicinal Chemistry, 124,* 417–427.
28. Qin, Q.-P., Qin, J.-L., Meng, T., Lin, W.-H., Zhang, C.-H., et al. (2016). High in vivo antitumor activity of cobalt oxoisoaporphine complexes by targeting g-quadruplex DNA, telomerase and disrupting mitochondrial functions. *European Journal of Medicinal Chemistry, 124,* 380–392.
29. Qin, Q.-P., Qin, J.-L., Meng, T., Yang, G.-A., Wei, Z.-Z., et al. (2016). Preparation of 6/8/11-amino/chloro-oxoisoaporphine and group-10 metal complexes and evaluation of their in vitro and in vivo antitumor activity. *Scientific Reports, 6,* 37644.
30. Huang, L., Luo, Y., Pu, Z., Kong, X., Fu, X., et al. (2017). Oxoisoaporphine alkaloid derivative 8–1 reduces aβ1-42 secretion and toxicity in human cell and caenorhabditis elegans models of Alzheimer's disease. *Neurochemistry International, 108,* 157–168.
31. Tang, H., Zhao, L.-Z., Zhao, H.-T., Huang, S.-L., Zhong, S.-M., et al. (2011). Hybrids of oxoisoaporphine-tacrine congeners: novel acetylcholinesterase and acetylcholinesterase-induced β-amyloid aggregation inhibitors. *European Journal of Medicinal Chemistry, 46,* 4970–4979.
32. Wei, S., Chen, W., Qin, J., Huangli, Y., Wang, L., et al. (2016). Multitarget-directed oxoisoaporphine derivatives: anti-acetylcholinesterase, anti-β-amyloid aggregation and enhanced autophagy activity against Alzheimer's disease. *Bioorganic and Medicinal Chemistry, 24,* 6031–6039.
33. Sobarzo-Sánchez, E., Bilbao-Ramos, P., Dea-Ayuela, M., González-Díaz, H., Yañez, M., et al. (2013). Synthetic oxoisoaporphine alkaloids: in vitro, in vivo and in silico assessment of antileishmanial activities. *PLoS ONE, 8,* e77560.
34. Rosquete, L. I., Cabrera-Serra, M. G., Piñero, J. E., Martín-Rodríguez, P., Fernández-Pérez, L., et al. (2010). Synthesis and in vitro antiprotozoal evaluation of substituted phenalenone analogues. *Bioorganic and Medicinal Chemistry, 18,* 4530–4534.
35. Tang, H., Wei, Y.-B., Zhang, C., Ning, F.-X., Qiao, W., et al. (2009). Synthesis, biological evaluation and molecular modeling of oxoisoaporphine and oxoaporphine derivatives as new dual inhibitors of acetylcholinesterase/butyrylcholinesterase. *European Journal of Medicinal Chemistry, 44,* 2523–2532.
36. Ning, F. X., Weng, X., Huang, S. L., Gu, L. J., Huang, Z. S., et al. (2011). A facile and efficient method for hydroxylation of azabenzanthrone compounds. *Chinese Chemical Letters, 22,* 41–44.
37. Wang, Y., Wang, Q., Zhang, H., Wu, Y., Jia, Y., et al. (2020). CTAB-assisted solvothermal construction of hierarchical Bi_2MoO_6/Bi_5O_7Br with improved photocatalytic performances. *Separation and Purification Technology, 242,* 116775.
38. Jia, Y., Liu, P., Wang, Q., Wu, Y., Cao, D., et al. (2021). Construction of Bi_2S_3-BiOBr nanosheets on TiO_2 NTA as the effective photocatalysts: pollutant removal, photoelectric conversion and hydrogen generation. *Journal of Colloid and Interface Science, 585,* 459–469.
39. Wang, Q., Li, H., Yu, X., Jia, Y., Chang, Y., et al. (2020). Morphology regulated Bi_2WO_6 nanoparticles on TiO_2 nanotubes by solvothermal Sb^{3+} doping as effective photocatalysts for wastewater treatment. *Electrochimica Acta, 330,* 135167.
40. Cao, D., Wang, Q., Wu, Y., Zhu, S., Jia, Y., et al. (2020). Solvothermal synthesis and enhanced photocatalytic hydrogen production of Bi/Bi_2MoO_6 co-sensitized TiO_2 nanotube arrays. *Separation and Purification Technology, 250,* 117132.
41. Ando, K., & Fujita, T. (2009). Metabolic syndrome and oxidative stress. *Free Radical Biology and Medicine, 47,* 213–218.
42. Xie, L., Zhu, X., Hu, Y., Li, T., Gao, Y., et al. (2008). Mitochondrial DNA oxidative damage triggering mitochondrial dysfunction and apoptosis in high glucose-induced HRECs. *Investigative Ophthalmology and Visual Science, 49,* 4203–4209.